Scripta Materialia 255 (2025) 116401

Contents lists available at ScienceDirect

Scripta Materialia

journal homepage: www.journals.elsevier.com/scripta-materialia

Stress increase by nanoscale hcp precipitates in HfNbTaTiZr high entropy alloys

Hiroyuki Y. Yasuda [a,*], Yusuke Yamada [a], Masato Onishi [a], Hiroki Suzuki [a], Ken Cho [a], Satoshi Ichikawa [b], Takeshi Nagase [c]

[a] Division of Materials and Manufacturing Science, Graduate School of Engineering, Osaka University, 2-1, Yamada-oka, Suita, Osaka, 565-0871, Japan
[b] Research Center for Ultra-High Voltage Electron Microscopy, Osaka University, 7-1, Mihogaoka, Ibaraki, Osaka, 567-0047, Japan
[c] Department of Materials and Synchrotron Radiation Engineering, Graduate School of Engineering, University of Hyogo, 2167, Shosha, Himeji, Hyogo, 671-2280, Japan

ARTICLE INFO

Keywords:
High entropy alloys
Refractory metals
Plastic deformation
Phase transformation
Spinodal decomposition

ABSTRACT

HfNbTaTiZr high entropy alloys show a stress increase around 873 K, especially in the single crystals. At 873 K, the bcc single phase is decomposed into the bcc1 and bcc2 phases due to spinodal decomposition with composition modulation along ⟨100⟩ direction. The bcc1 phase has Zr- and Hf-rich composition, while Nb and Ta are enriched in the bcc2 phase. Next, the hcp phase is precipitated along the bcc1 phase. As a result, the hcp phase is aligned parallel to {100} plane of the bcc phase. The fine hcp phase acts as a strong barrier to the dislocation motion, resulting in the stress increase at 873 K.

High entropy alloys (HEA) composed of five or more elements of which concentrations are 5–35 % have attracted much attention due to their high strength and good resistance to severe environment and radiation [1–4]. In particular, HEA with refractory elements such as Mo, Nb, Ta, etc. are called refractory high entropy alloys (RHEA) and are expected to be a potential candidate for high temperature structural materials [5–8]. HfNbTaTiZr alloys which is a typical RHEA, first proposed by Senkov et al., show high strength at high temperatures and can be heavily cold rolled to 86 % [9–12]. In our previous paper, we investigated the deformation behavior of HfNbTaTiZr single crystals and polycrystals [13]. As a result, the yield stress decreases rapidly with increasing temperature up to 673 K, which is similar to bcc metals. On the other hand, the yield stress significantly increases around 873 K. Especially, in the single crystals, a stress increase between 673 K and 873 K is 560 MPa. Since the hcp phase is found to be precipitated around 873 K, the formation of the hcp phase seems to be closely related to the stress increase [13]. However, the detailed mechanism of the stress increase is still unclear. Thus, in the present study, the mechanism of the stress increase at 873 K in HfNbTaTiZr alloys was discussed based on the microstructure observation after deformation. Consequently, a spinodal decomposition of the bcc phase followed by the formation of the hcp phase is found to play an important role in an abnormal increase in yield stress around 873 K.

The preparation method for equiatomic HfNbTaTiZr single crystals and polycrystals is described in a previous paper [13]. The single crystals were solutionized at 1473 K for 1 h followed by water cooling. In order to examine the effect of microstructure change on strength, micro-Vickers hardness was measured for the single crystals solutionized at 1473 K and then annealed at 873 K. The indentation plane is (530). The rectangular specimens of which dimension is 2 × 2 × 5 mm were compressed to 1 % at 873 K in vacuum with $[\bar{1}68]$ orientation at a cross-head speed of 0.05 mm/min which corresponds to an initial strain rate of 1.7×10^{-4} /s (condition (I)). Note that the compression tests were conducted using a conventional test machine with an electric heat furnace. In order to stabilize the temperature in the furnace, the holding time at the test temperature before the compression tests was set to 1800s. The microstructure after deformation was observed using a transmission electron microscope (TEM) operated at 300 kV and a high angle annular dark field-scanning transmission electron microscope (HAADF-STEM, JEOL JEM-ARM200F) equipped with energy dispersive X-ray spectroscopy (EDS) detector. The thin foils for TEM and HAADF-STEM observation were perforated by an Ar ion milling. Subscripts for directions and planes on TEM and HAADF-STEM analysis mean the corresponding phase. In order to examine the effect of holding time at the compression test temperature, Gleeble-type test machine with an induction furnace was also used to minimize the holding time. In addition, a strain rate was increased to suppress the formation of the hcp phase during compression. The compression tests were also conducted

* Corresponding author.
E-mail address: hyyasuda@mat.eng.osaka-u.ac.jp (H.Y. Yasuda).

https://doi.org/10.1016/j.scriptamat.2024.116401
Received 24 June 2024; Received in revised form 23 August 2024; Accepted 25 September 2024
Available online 1 October 2024

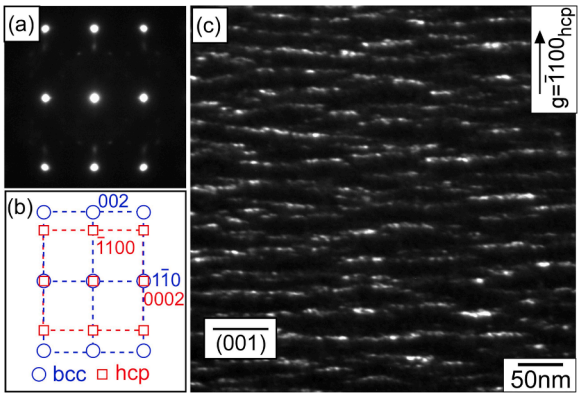

Fig. 1. A SAEDP (a) and a dark-field image with $g = \bar{1}100_{hcp}$ (c) in HfNbTaTiZr single crystals compressed at 873 K under condition (I). (b) A schematic illustration of (a). (a), (b) beam direction (*B*) is $[110]_{bcc}$, $[11\bar{2}0]_{hcp}$.

under the following two conditions. Since the large single crystals for Gleeble-type test machine could not be obtained, the tests were done using the polycrystals. Condition (II): Conventional compression test machine with an electric heat furnace was used. In order to stabilize the temperature in the furnace, the holding time at the test temperature before the compression test was set to 1800s. A high strain rate of 1.7×10^{-2} /s was selected to suppress the formation of the hcp phase. Condition (III): Gleeble-type test machine with an induction heat furnace was used. High heating rate (10 K s^{-1}) and short holding time before the compression test (120 s) were realized at 873 and 1073 K. A high strain rate of 1.7×10^{-2} /s was also chosen to suppress the formation of the hcp phase.

Fig. 1(a), (b) shows a selected area diffraction pattern (SAEDP) of HfNbTaTiZr single crystals compressed at 873 K under condition (I). $[110]_{bcc}$ pattern of the bcc matrix can be observed, while $[11\bar{2}0]_{hcp}$ pattern of the hcp phase can also be seen. A dark-field image with a reflection vector (g) of $\bar{1}100_{hcp}$ of the hcp phase is shown Fig. 1(c). While dots are aligned parallel to $\{001\}_{bcc}$ plane of the bcc phase, suggesting that the hcp phase is densely precipitated along $\{001\}_{bcc}$ plane. It is also noted that the size of the hcp precipitates is <10 nm. It is well known that in Ti alloys, the bcc and the hcp phases satisfy the Burgers orientation relationship $\{110\}_{bcc}//\{0001\}_{hcp}$, $<111>_{bcc}//<1120>_{hcp}$. However, the orientation relationship in HfNbTaTiZr alloys compressed at 873 K is $\{110\}_{bcc}//\{0001\}_{hcp}$, $<110>_{bcc}//<1120>_{hcp}$. Fig. 2 shows STEM-EDS maps (b)-(f) together with the HAADF image (a) of the crystals compressed at 873 K under condition (I). In the HAADF image (Fig. 2(a)), there are bright and dark regions mainly composed of heavy and light elements, respectively. In fact, from the EDS maps, Nb and Ta are enriched in the bright region (Fig. 2(c) and (d)), while the dark region has Hf- and Zr-rich composition (Fig. 2(b) and (f)). On the other hand, distribution of Ti is homogenous (Fig. 2(e)). In previous papers, the phase separation into two bcc phases is observed in HfNbTaTiZr alloys [13–15]. Moreover, in Zr-Nb binary alloy system, spinodal decomposition into two bcc phases is known to occur [16,17]. This strongly suggests that spinodal decomposition also takes place in HfNbTaTiZr alloys. Fig. 3(a) shows a high resolution TEM (HRTEM) image of the crystals compressed at 873 K under condition (I). Fig. 3(b) and (c) show fast Fourier transform (FFT) patterns taken from regions A and B in Fig. 3(a), respectively. Enlarged filtered inverse FFT (IFFT) images of Fig. 3(b) and (c) are shown in Fig. 3(d) and (e), respectively. Both the FFT patterns and IFFT images indicate that region A which corresponds to Nb, Ta-rich light region in Fig. 2(a) consists of the bcc phase. On the other hand, region B corresponding to Hf, Zr-rich dark region in Fig. 2(a) is composed of the hcp phase. This strongly suggests that the spinodal decomposition into Hf, Zr-rich and Nb, Ta-rich bcc phases (referred to as bcc1 and bcc2 phases, respectively [13]) occurs and then the hcp phase is precipitated from the bcc1 phase, which is schematically illustrated in Fig. 3(f). In fact, the lattice plane spacings shown in Fig. 3(d) and (e) are consistent with those of the bcc2 and the

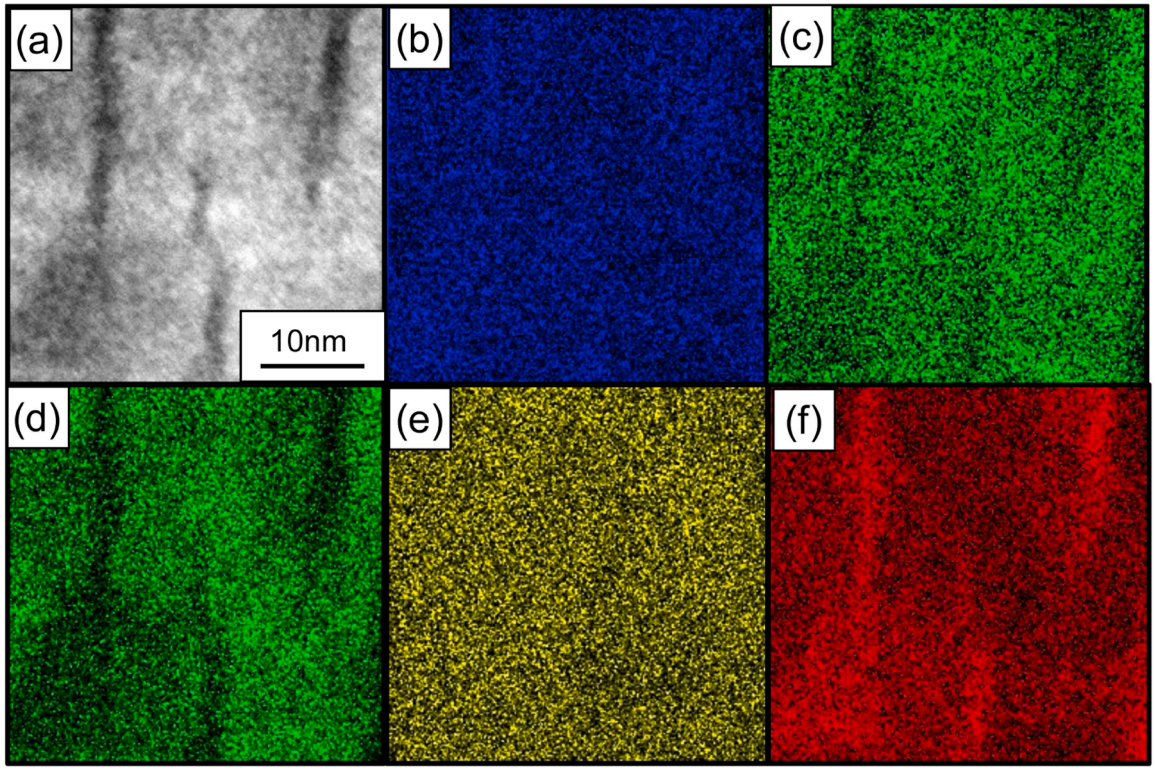

Fig. 2. A HAADF-STEM image (a) and STEM-EDS maps (b)–(f) in HfNbTaTiZr single crystals compressed at 873 K under condition (I); (b) Hf, (c) Nb, (d) Ta, (e) Ti and (f) Zr.

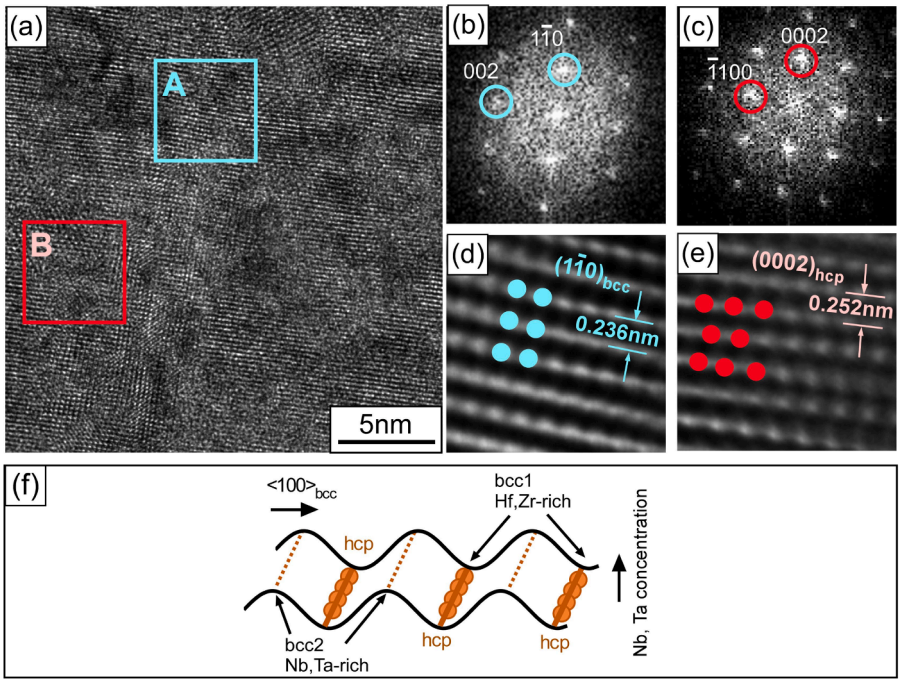

Fig. 3. (a) A HRTEM image of HfNbTaTiZr single crystals compressed at 873 K under condition (I); taken along $[110]_{bcc}$ and $[11\bar{2}0]_{hcp}$ directions. FFT patterns from regions A (b) and B (c) in (a). Regions A and B are composed of the bcc and hcp phases, respectively. (d) and (e) Enlarged filtered IFFT images of (b) and (c), respectively. (f) A schematic illustration of the spinodal decomposition into the bcc1 and bcc2 phases, followed by the precipitation of the hcp phase.

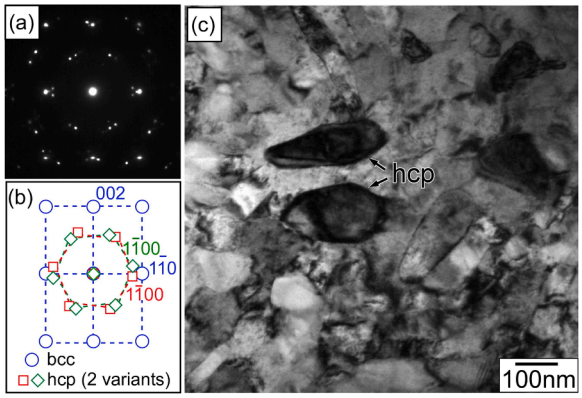

Fig. 4. A SAEDP (a) and a bright field image (c) of HfNbTaTiZr alloys annealed at 873 K for 100 h. (b) a schematic drawing of (a); $B = [110]_{bcc}$, $[0001]_{hcp}$. At least two hcp variants can be seen.

hcp phase, respectively [13]. The orientation relationship between the bcc and the hcp phases in Fig. 3 is $\{110\}_{bcc}//\{0001\}_{hcp}$, $<110>_{bcc}//<1120>_{hcp}$, which is consistent with Fig. 1. For comparison, HfNbTaTiZr alloys was annealed at 873 K for 100 h and the microstructure is shown in Fig. 4. There exists numerous precipitates with the hcp structure in the bcc matrix (Fig. 4(c)) and the SAEDP (Fig. 4(a) and (b)) suggests that at least two variants of the hcp phase are precipitated satisfying the Burgers orientation relationship with the bcc matrix.

In the present study, spinodal decomposition of the bcc phase into Hf, Zr-rich bcc1 and Nb, Ta-rich bcc2 phases occurs at 873 K, followed by the transformation from the bcc1 to the hcp phase. The phase transformation behavior of HfNbTaTiZr alloys is similar to that of Zr-Nb binary alloy system [16,17]. The phase separation of the bcc phase and the precipitation of the hcp and the ω phases take place in HfNbTaTiZr alloys [13–15]. Some researchers also reported the spinodal decomposition of the bcc phase into the bcc1 and bcc2 phases in bcc HEA [18-20]. Flewitt [16] and Toda et al. [17] reported that the successive phase transformation composed of the spinodal decomposition and the hcp precipitation occurs in Zr-Nb alloys below the monotectoid temperature around 900 K. Since the wavelength of composition modulation accompanied by the spinodal decomposition is about 10 nm, the hcp phase precipitated from the Hf, Zr-rich bcc1 phase is densely precipitated, as shown in Fig. 1. In Fig. 1, the hcp phase shows a dotted contrast. This means that the band region except the hcp phase is the Hf, Zr-rich bcc1 phase. It is also noted that the direction of composition modulation in bcc metals is $<100>_{bcc}$, resulting in the alignment of the hcp phase on $\{100\}_{bcc}$ plane, as shown in Figs. 1 and 3(f). In other words, if the hcp phase is precipitated before the spinodal decomposition, the hcp phase does not have to be aligned parallel to $\{100\}_{bcc}$ plane. Fig. 5(a) shows variation in micro-Vickers hardness with annealing time in the single crystals solutionized and then annealed at 873 K. The hardness increases rapidly with increasing annealing time and shows a high value even after annealing for 0.2 h. This means that the spinodal decomposition proceeds rapidly during the holding time at 873 K before and during the compression tests. The hcp phase formed by the transformation from the bcc1 phase is so fine and densely distributed that the dislocation motion in the alloys is strongly suppressed by the hcp phase. This results in the stress increase around 873 K in HfNbTaTiZr alloys [13]. In order to examine the effect of holding time at 873 K, the compression tests were also conducted using Gleeble-type test machine equipped with induction heat furnace, which can realize high heating rate and short holding time at the test temperature. Fig. 5(b) shows temperature dependence of yield stress of HfNbTaTiZr polycrystals compressed under conditions (II) and (III). The data for the single crystals and polycrystals compressed under condition (I) are also shown in the figure [13]. Under conditions (I) and (II), a stress increase can be seen at 873 K, especially in the single crystals. In addition, under condition (I), the single crystals and polycrystals demonstrate similar temperature dependence of yield stress except 873 K. Since the grain size of the polycrystals is about 500 μm, the effect of grain boundaries on the strength is insignificant. Moreover, the yield stress of the polycrystals under condition (II) is higher than that under condition (I), since the deformation behavior of bcc metals generally depends strongly on strain rate [13]. On the other hand, the

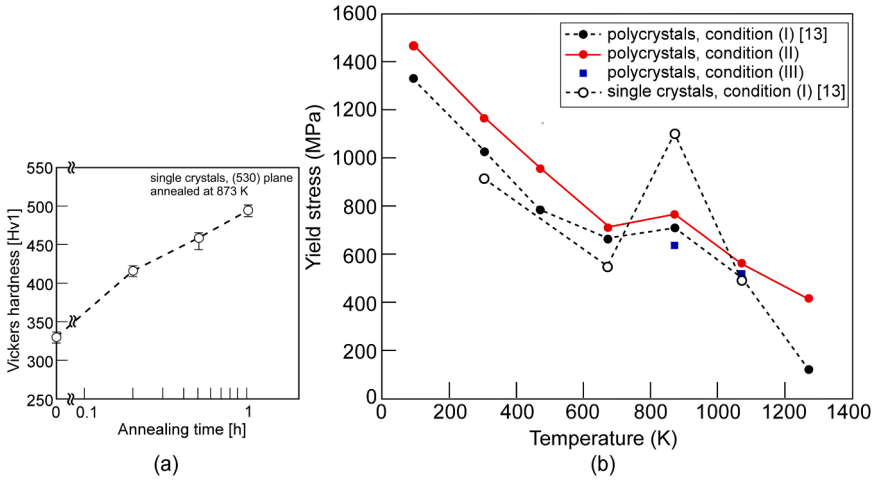

Fig. 5. (a) Variation in micro-Vickers hardness with annealing time in HfNbTaTiZr single crystals solutionized at 1473 K and then annealed at 873 K. (b) Temperature dependence of yield stress of HfNbTaTiZr polycrystals compressed under conditions (II) and (III). The data for the single crystals and polycrystals compressed under condition (I) are also shown [13].

stress increase at 873 K becomes insignificant under condition (III) using Gleeble-type test machine, as shown in Fig. 5(b). This suggests that the hcp phase is hardly formed during short holding time under condition (III). Thus, one can conclude that the successive phase transformation leading to the hcp nanoprecipitates is responsible for the stress increase around 873 K in HfNbTaTiZr alloys. On the other hand, at 1073 K, the hcp phase is never precipitated, although the phase decomposition of the bcc phase takes place [13]. From the calculated phase diagram, the hcp phase can be precipitated below 1073 K [5]. Stress increase is not significant at 1073 K, suggesting that the phase decomposition of the bcc phase is not responsible for strong hardening. It is also noted that the stress increase by the formation of the hcp phase is more remarkable in the single crystals, compared with the polycrystals [13]. In the case of the polycrystals, the bcc2 phase which has Nb, Ta-rich composition is formed along the boundaries of the bcc matrix grains [13–15]. In this case, a driving force for the spinodal decomposition in the bcc grain interior decreases, which leads to slow precipitation of the hcp phase and a weak stress increase in the polycrystals. In fact, micro-Vickers hardness of the single crystals increases more rapidly with increasing annealing time at 873 K than that of the polycrystals [13]. In addition, the grain size of the polycrystals is nearly 500 μm, grain boundary strengthening effect is not significant. It is also noted that the bcc and hcp phases satisfy $\{110\}_{bcc}//\{0001\}_{hcp}$, $<110>_{bcc}//<1120>_{hcp}$ orientation relationship in the deforming crystals instead of the Burgers one. In general, spinodal decomposition accompanies strong stress field, resulting in the deviation from the Burgers relationship. On the other hand, if the alloys are annealed at 873 K for long time, the Burgers orientation relationship holds between the bcc and hcp phases, as shown in Fig. 4.

In HfNbTaTiZr alloys, the yield stress is increased around 873 K, especially in the single crystals. The spinodal decomposition from the bcc matrix into the bcc1 and bcc2 phases occurs rapidly and then subsequently the nanoscale hcp phase is precipitated from the bcc1 phase. Numerous hcp precipitates along $\{100\}_{bcc}$ plane of the bcc matrix strongly suppress the dislocation motion, resulting in the stress increase.

CRediT authorship contribution statement

Hiroyuki Y. Yasuda: Writing – original draft, Supervision, Methodology, Investigation, Funding acquisition, Formal analysis, Data curation, Conceptualization. **Yusuke Yamada:** Writing – review & editing, Investigation, Formal analysis, Data curation. **Masato Onishi:** Writing – review & editing, Investigation, Formal analysis, Data curation. **Hiroki Suzuki:** Writing – review & editing, Visualization, Investigation, Formal analysis, Data curation. **Ken Cho:** Writing – review & editing, Investigation, Formal analysis, Data curation. **Satoshi Ichikawa:** Writing – review & editing, Investigation, Formal analysis, Data curation. **Takeshi Nagase:** Investigation, Formal analysis, Data curation.

Declaration of competing interest

The authors declare that they have no known competing financial interests or personal relationships that could have appeared to influence the work reported in this paper.

Acknowledgment

This work was supported by a Grant-in Aid for Challenging Research (Exploratory) (grant no. 18K18949) from the Japan Society for the Promotion of Science (JSPS).

References

[1] B. Cantor, I.T.H. Chang, P. Knight, A.J.B. Vincent, Microstructural development in equiatomic multicomponent alloys, Mater. Sci. Eng. A. 375–377 (2004) 213–218.
[2] B.S. Murty, J.-W. Yeh, S. Ranganathan, High-Entropy Alloys, Elsevier, Amsterdam, 2014.
[3] (eds.)M.C. Gao, J-W. Yeh, P.K. Liaw, Y. Zhang (Eds.), High-Entropy Alloys: Fundamentals and Applications, Springer, Cham, 2016.
[4] Y. Zhang, T.T. Zuo, Z. Tang, M.C. Gao, K.A. Dahmen, P.K. Liaw, Z.P. Lu, Microstructures and properties of high-entropy alloys, Prog. Mater. Sci. 61 (2014) 1–93.
[5] M.C. Gao, C.S. Carney, N. Doğan, P.D. Jablonksi, J.A. Hawk, D.E. Alman, Design of refractory high-entropy alloys, JOM 67 (2015) 2653–2669.
[6] D.B. Miracle, O.N. Senkov, A critical review of high entropy alloys and related concepts, Acta Mater. 122 (2017) 448–511.
[7] O.N. Senkov, D.B. Miracle, K.J. Chaput, J.-P. Couzinie, Development and exploration of refractory high entropy alloys—a review, J. Mater. Res. 33 (2018) 3092–3128.
[8] O.N. Senkov, G.B. Wilks, D.B. Miracle, C.P. Chuang, P.K. Liaw, Refractory high-entropy alloys, Intermetallics 18 (2010) 1758–1765.
[9] O.N. Senkov, J.M. Scott, S.V. Senkova, D.B. Miracle, C.F. Woodward, Microstructure and room temperature properties of a high-entropy TaNbHfZrTi alloy, J. Alloy. Compd. 509 (2011) 6043–6048.
[10] O.N. Senkov, J.M. Scott, S.V. Senkova, F. Meisenkothen, D.B. Miracle, C. F. Woodward, Microstructure and elevated temperature properties of a refractory TaNbHfZrTi alloy, J. Mater. Sci. 47 (2012) 4062–4074.
[11] O.N. Senkov, S.L. Semiatin, Microstructure and properties of a refractory high-entropy alloy after cold working, J. Alloy. Compd. 649 (2015) 1110–1123.
[12] G. Dirras, J. Gubicza, A. Heczel, L. Lilensten, J.-P. Couzinié, L. Perrière, I. Guillot, A. Hocini, Microstructural investigation of plastically deformed Ti20Zr20Hf20Nb20Ta20 high entropy alloy by X-ray diffraction and transmission electron microscopy, Mater. Charact. 108 (2015) 1–7.

[13] H.Y. Yasuda, Y. Yamada, K. Cho, T. Nagase, Deformation behavior of HfNbTaTiZr high entropy alloy singe crystals and polycrystals, Mater. Sci. Eng. A 809 (2021) 140983.
[14] N.D. Stepanov, N.Y. Yurchenko, S.V. Zherebtsov, M.A. Tikhonovsky, G. A. Salishchev, Aging behavior of the HfNbTaTiZr high entropy alloy, Mater. Lett. 211 (2018) 87–90.
[15] S.Y. Chen, Y. Tong, K.K. Tseng, J.W. Yeh, J.D. Poplawsky, J.G. Wen, M.C. Gao, G. Kim, W. Chen, Y. Ren, R. Feng, W.D. Li, P.K. Liaw, Phase transformations of HfNbTaTiZr high-entropy alloy at intermediate temperatures, Scr. Mater. 158 (2019) 50–56.
[16] P.E.J. Flewitt, Phase transformations in niobium 16 to 40% zirconium alloys below the monotectoid temperature–II, Acta Metall. 22 (1974) 65–79.
[17] Y. Toda, H. Nakagawa, T. Koyama, T. Miyazaki, An analysis of the phase decomposition in Nb-Zr alloy based on the system free energy theory, Mater. Sci. Eng. A. 255 (1998) 90–97.
[18] Y. Zhou, S. Zeng, H. Li, H. Zhang, H. Zhang, Z. Zhu, A design of Zr-rich body-centered cubic structured refractory complex concentrated alloy with outstanding tensile strength and ductility, Mater. Sci. Eng. A. 874 (2023) 145091.
[19] T. Xiang, M. Zhao, P. Du, G. Xie, Heat treatment effects on microstructure and mechanical properties of TiZrNbTa high-entropy alloy, J. Alloy. Compd. 930 (2023) 167408.
[20] T. Li, S. Wang, W. Fan, Y. Lu, T. Wang, T. Li, P.K. Liaw, CALPHAD-aided design for superior thermal stability and mechanical behavior in a TiZrHfNb refractory high-entropy alloy, Acta Mater. 246 (2023) 118728.